Water Science & Technology

Water Science & Technology Vol 87 No 1, 144 doi: 10.2166/wst.2022.420

Improvement of coal gasification reverse osmosis concentrate treatment by Cu-Co-Mn/AC catalytic ozonation

Xiurong Chen [a,b,*], Hao Gu[a], Xiaoli Sun[c], Jinyi Tian[a], Qiuyue Li[a], Tao Pan[a], Xinyu Zhang[a], Xueyang Hu[a] and Shanshan Linghu[a]

[a] National Engineering Research Center of Industrial Wastewater Detoxication and Resource Recovery, East China University of Science and Technology, Shanghai 200237, China
[b] State Environmental Protection Key Laboratory of Environmental Risk Assessment and Control on Chemical Process, East China University of Science and Technology, Shanghai 200237, China
[c] Shanghai Municipal Engineering Design Institute (Group) Co., LTD, Shanghai 200082, China
*Corresponding author. E-mail: xrchen@ecust.edu.cn

XC, 0000-0003-2544-6570

ABSTRACT

Approximately 20% of concentrate will be produced from coal gasification wastewater after reverse osmosis treatment. The organic matter contained in the concentrate affects its evaporation crystallisation; therefore, the refractory organics must be removed. In this study, Cu-Co-Mn/AC catalytic ozonation was used to treat reverse osmosis concentrate (ROC). With the addition of the Cu-Co-Mn/AC catalyst, the production of ·OH increased by 82 μmol/L, thereby enhancing the ozonation performance. The pH, ozone dosage, and catalyst dosage all affected the catalytic ozonation performance. By constructing a response surface model, it was found that the catalyst dosage had the most significant effect on the catalytic ozonation performance. The predicted optimal reaction conditions were pH = 9.02, ozone dosage = 1.08 g/L, and catalyst dosage = 1.33 g/L, under which the chemical oxygen demand (COD) removal reached a maximum of 81.49%.

Key words: catalytic ozonation, response surface model, reverse osmosis concentrate (ROC), zero liquid discharge

HIGHLIGHTS

- The Cu-Co-Mn/activated carbon catalyst enhanced the ozonation efficiency for treating reverse osmosis concentrate (ROC).
- The removal of COD from ROC by catalytic ozonation could be about 80%.
- A response surface model was established to determine the operating parameters of catalytic ozonation.

1. INTRODUCTION

Similar to other coal chemical processes, coal gasification produces a large amount of wastewater (Yang *et al.* 2021). Reverse osmosis has been widely used for the treatment and reuse of coal chemical wastewater (Li *et al.* 2020). However, the process produces a concentrate of 15–30% (Westerhoff *et al.* 2009; Chen *et al.* 2020) containing high quantities of Na^+, Ca^{2+}, Mg^{2+}, Cl^-, and SO_4^{2-} (Wang *et al.* 2021). To achieve 'zero liquid discharge' of coal chemical wastewater, the reverse osmosis concentrate (ROC) must be further treated.

At present, 60% of domestic ROC treatment projects use the evaporation crystallisation process (Shi *et al.* 2020). However, in addition to containing a high quantity of salts, ROC also contains many organic matters, such as phenol, hydroquinone, quinoline, and isoquinoline (Zhu *et al.* 2018). The presence of refractory organics in the concentrate significantly affects the evaporation crystallisation processes and the salt quality (Jia *et al.* 2017). However, traditional organic treatment methods have many shortcomings. For example, high salinity will affect the chemical hydrolysis of the coagulant and the dissolution of metal hydroxides; thus, the removal of COD in the concentrate by coagulation precipitation is only 20–40% (Liu *et al.* 2019). Additionally, ROC has strong biological toxicity and poor biodegradability (B/C = 0.03–0.05), which limits the application of the activated sludge method (Hou *et al.* 2020). Fenton oxidation produces a large amount of iron-rich sludge, resulting in high treatment costs (Yang *et al.* 2020), and electrochemical oxidation produces trichloromethane and other

disinfection by-products when used to treat chlorine-containing concentrates, causing secondary pollution (Keyikoglu *et al.* 2021). Therefore, a new process that can efficiently remove organic matter from ROC must be urgently developed.

Catalytic ozonation has been used in a variety of wastewater treatment fields due to its extremely mature application system and has exhibited an excellent degradation efficiency (Araújo *et al.* 2021; Li *et al.* 2021). Ozone decomposes to generate free radicals through the promotion of active components on the catalyst to achieve non-selective oxidative organic matter (Nawrocki & Kasprzyk-Hordern 2010). He *et al.*(2020) used catalytic ozonation to treat coking wastewater, effectively reducing the COD of biologically treated effluent from 150 to 78 mg/L. Zhou *et al.* (2020) used MgO/AC catalytic ozonation to treat phenol in water, and the phenol and COD removal reached 88.5% and 83.5%, respectively. Nakhate *et al.* (2019) used Cu-doped ZnO catalytic ozonation to treat textile wastewater, and the COD removal reached 89%. The pH, ozone dosage, and catalyst dosage are all key factors affecting the generation and extinction of free radicals in catalytic ozonation systems (Luo *et al.* 2020; Yuan *et al.* 2020; Chen & Wang 2021). However, few studies have been conducted on the treatment of coal chemical ROC by catalytic ozonation under optimal conditions, including the pH, ozone dosage, and catalyst dosage.

In this study, Cu-Co-Mn/AC catalytic ozonation was used to treat a coal gasification ROC. The COD removal and ·OH real-time concentration were then compared to investigate the influence of the Cu-Co-Mn/AC catalyst on the ozonation system. The pH, catalyst dosage, and ozone dosage were regulated to determine the effect of operating conditions on the performance of the catalytic ozonation, and a response surface model (RSM) was used to determine the appropriate operating conditions, providing a reference for practical applications.

2. MATERIALS AND METHODS

2.1. Materials and reagents

All reagents were of analytical grade. The simulated wastewater was a simulated ROC of coal gasification wastewater after coagulation treatment. The composition of the simulated solution is listed in Table 1. $COD_{Cr} = 172.3$ mg/L, pH = 7.75.

2.2. Catalyst preparation

The catalyst was prepared by impregnation, and the main processes included pre-treatment, impregnation, drying, and calcination. The diagram for Cu-Co-Mn/AC catalyst preparation was shown in Figure 1, and the experimental scheme was as follows: 6 g of activated carbon was soaked in 1 mol/L sodium hydroxide solution and 0.1 mol/L dilute hydrochloric acid successively and stirred for 1 h. The solid was taken out and washed with deionized water to obtain the pre-treated activated carbon matrix. A mixed metal salt solution (Cu: Co: Mn = 1: 1: 1) with a concentration of 2.6 mol/L was prepared. The

Table 1 | Water quality analysis table

Ingredient	Concentration (mg/L)	Ingredient	Concentration (mg/L)
Isopropyl stearate	0.45	3-(Methylamino)phenol	1.51
Diisooctyl phthalate	1.32	Octadecane	0.49
Methyl 3-(Trimethylsilyl)propiolate	13.62	1,2-Bis(trimethylsilyl)benzene	0.34
4-(1-Methyl-1H-imidazol-5-yl) piperidine	6.76	Methylmaleic hydrazide	0.61
2,3,6-Trichlorobiphenyl	5.50	Catechol	4.54
5-Methyl-2-Hexanone oxime	1.33	Resorcinol	4.54
1-Tridecanol	0.52	Hydroquinone	4.54
1-(2-Methoxyethoxy)-2-Methyl-2-Propanol	0.71	Pyridine	12.73
Stearic acid	2.97	Indole	6.45
2-Isonitroacetophenone	0.24	Quinoline	6.45
Octadecanamide	0.20	Sodium chloride	2,600
Acetamide	0.49	Sodium sulphate	2,400
Decyl Ether	0.53	Sodium nitrate	800
1-Octadecene	0.35	Calcium chloride	110
Purine	0.86	Potassium chloride	64

Figure 1 | The diagram for Cu-Co-Mn/AC catalyst preparation.

activated carbon matrix was immersed in the mixed metal salt solution and stirred for 2 h. The impregnated solid was dried at 105 °C for 12 h, and finally calcined at 600 °C for 4.5 h. After cooling down, the Cu-Co-Mn/AC catalyst was obtained.

2.3. Catalytic ozonation system setup

In the catalytic ozonation system, ozone dissolved in the liquid phase is transferred to the catalyst's surface, and the organic contaminants and ozone are both adsorbed onto the catalyst's surface. Free radical reactions undergo at the active sites on the surface of the metal oxide. The free active species generated, such as ·OH, would attack the organic pollutants or react with ozone to generate more ·OH (Nawrocki & Kasprzyk-Hordern 2010).

Figure 2 presents a diagram of the device used for the catalytic ozone oxidation reaction in this study. The experimental process was as follows: 3 L of the simulated solution was fed into the reactor. Dilute hydrochloric acid and sodium hydroxide were used to adjust the initial pH of the simulated solution. The catalyst was packed into the filler plate with 1.8 g, 2.7 g, 3.6 g, 4.5 g, and 5.4 g, respectively. Ozone gas was produced by an ozone generator (Model: JY-SY20, Jinyuan Ozone Co., Ltd) and the ozone concentration was measured by an ozone concentration detector (Model: 3S-J5000, Tonglin Ozone Co., Ltd). The ozone flow rate was maintained at 1 L/min, and the ozone concentration in the feed gas was 20 mg/L, 35 mg/L, 50 mg/L, 65 mg/L, and 80 mg/L, respectively. The stirrer was switched on, and the filler plate rotated with the stirrer and came into full contact with the ozone and organic molecules in the solution. The experimental time was 60 min, and the unreacted ozone was discharged through a vent ozone destructor.

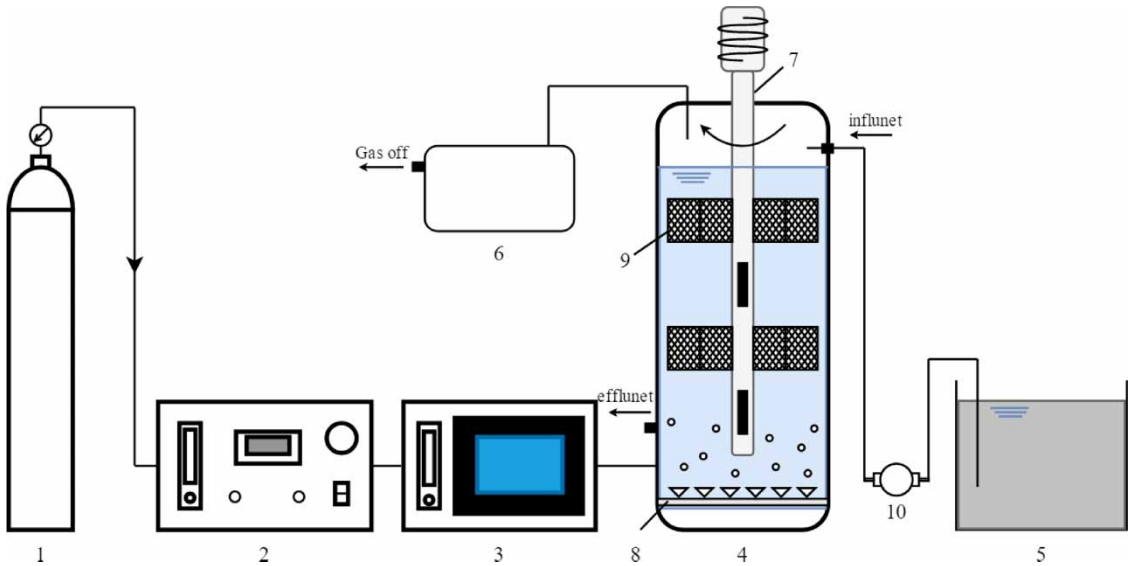

Figure 2 | Catalytic ozonation experimental device. (1: oxygen cylinder; 2: ozone generator; 3: ozone concentration detector; 4: reactor, 5: wastewater tank, 6: vent ozone destructor, 7: stirrer, 8: micropore aerator, 9: filler plate, 10: pump).

2.4. Analytical methods

Scanning electron micrograph (SEM) images of the AC and Cu-Co-Mn/AC catalysts were obtained from the Hitachi VP-SEM equipment (SU1510, Japan). The elemental compositions of these samples were analyzed by inductively coupled plasma optical emission spectrometer (ICP-OES) (Varian 710-ES, USA).

The COD of the solution was measured using a HACH instrument (DR200, USA; DR3900, USA), and a blank sample was prepared from deionised water. The concentration of hydroxyl radicals in the solution was measured as described below (Huang *et al.* 2019). Formaldehyde was produced by the reaction between hydroxyl radicals and dimethyl sulfoxide (DMSO), and further reacted with 2,4-Dinitrophenylhydrazine (DNPH) to form stable HCHO-DNPH. The amount of HCHO-DNPH produced was determined by high-performance liquid chromatography (Eksigent nanoLC-1D plus, USA) and used to calculate the hydroxyl radical concentration.

3. RESULTS AND DISCUSSIONS

3.1. Characterisation of the Cu-Co-Mn/AC catalyst

Figure 3 showed the SEM images of the pre-treated AC and Cu-Co-Mn/AC catalysts. It could be seen in Figure 3(a) that the pre-treated AC had many clear pores whose sizes were generally smaller than 5 μm. Laminar convex surfaces were also formed in some areas, and these structures would increase the number of adsorption sites. In Figure 3(b), the surface and pores of Cu-Co-Mn/AC catalysts were uniformly distributed with many irregular fine particles, and these particles were presumed to be oxides of Cu, Co, and Mn. The void structure of AC was changed because the generated active fraction entered into the pores and caused particle build-up.

Table 2 showed the content of each element for pre-treated AC and Cu-Co-Mn/AC catalysts. After impregnation and calcination, Cu, Co, and Mn were detected in AC, and the mass percentages of Cu, Co, and Mn were 1.44%,1.29%, and 1.37%, respectively. It indicated that the active components were successfully loaded on the surface of AC.

3.2. Performance of the catalyst, ozonation alone, and ozonation with catalyst

Coal gasification ROC was treated by 'Cu-Co-Mn/AC', 'Ozone', and 'Cu-Co-Mn/AC + ozone', respectively. Experiments were performed under the same initial conditions with an ozone dosage of 1.0 g/L, a catalyst dosage of 1.2 g/L, and a pH of 9.0.

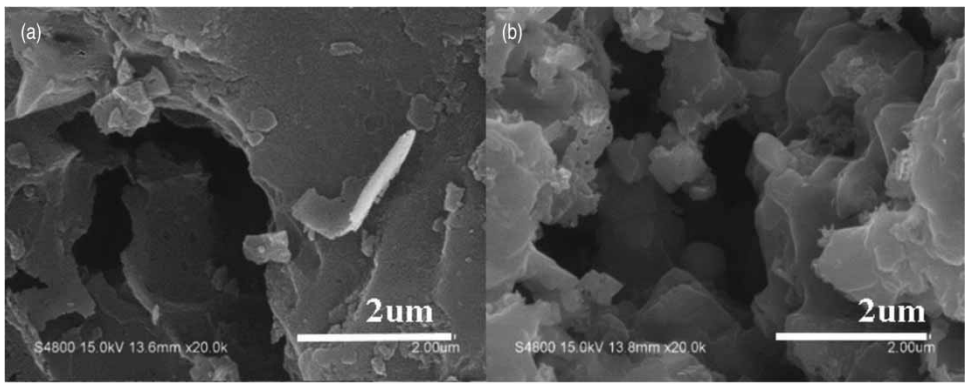

Figure 3 | The SEM images of the pre-treated AC and Cu-Co-Mn/AC catalysts.

Table 2 | Elements content of AC and Cu-Co-Mn/AC catalysts

Samples		C	O	Cu	Co	Mn	Others
AC	wt.%	94.21	5.71	0.00	0.00	0.00	0.08
Cu-Co-Mn/AC	wt.%	86.05	9.68	1.44	1.29	1.37	0.17

As shown in Figure 4, when the ROC was treated by the catalyst or ozonation alone, the removal of organic compounds in the ROC was poor. The COD removal was attributed to adsorption and oxidation reactions, respectively. The COD removal using ozonation alone was 1.66% higher than that using the catalyst alone, indicating that the oxidation reaction could better degrade organic matter than the adsorption reaction (Aldeguer Esquerdo *et al.* 2021; Liu *et al.* 2021).

The COD removal from the ROC was highest under Cu-Co-Mn/AC catalytic ozonation, exceeding 79%. The COD removal of the Cu-Co-Mn/AC catalytic ozonation were 60.8% and 59.14% higher than those of the catalyst and ozonation alone, respectively, and 40.02% higher than the sum of the COD removal of the individual processes. Many studies have demonstrated that catalysts can promote the decomposition of ozone to produce ·OH (Valdes & Zaror 2006). Figure 4 shows that the real-time concentration of ·OH production in the catalytic ozonation system was 82 μmol/L higher than that in the ozonation system. Cu-Co-Mn/AC catalysts increased the ·OH concentration of the ozone system by 6.8 times. The good COD removal performance of catalytic ozonation could be attributed to the generation of large amounts of ·OH. The addition of the Cu-Co-Mn/AC catalyst caused ozone to decompose and generate active ·OH, and the performance of ·OH in the oxidation of the organic matter in the ROC was stronger than that of ozonation alone. Therefore, the performance of the ozonation system with the Cu-Co-Mn/AC catalyst in COD removal was enhanced. Thus, it could be inferred that, in the Cu-Co-Mn/AC catalytic ozonation system, the contribution of each reaction to COD removal decreased in the following order: oxidation of hydroxyl radicals > direct ozone oxidation > catalyst adsorption. In the catalytic ozonation process, the pH, ozone dosage, and catalyst dosage all affect the amount of ·OH in the solution; therefore, further research on the above variables is required.

3.3. Effect of operating conditions on the catalytic ozonation performance

3.3.1. Effect of ozone dosage

As the reaction progressed, the COD removal of catalytic ozonation continuously increased. The degradation curve tended to be stable at the reaction time of 60 min, and the COD removal was related to the ozone dosage. As shown in Figure 5, at a relatively low ozone dosage, the amount of ·OH produced by ozone decomposition was low; therefore, the performance of catalytic ozonation for removing organic pollutants was poor. At this stage, the ozone dosage determined the amount of ·OH generated in the system. Meanwhile, an increase in ozone dosage may promote the mass transfer of ozone molecules into the aqueous solution and onto the catalyst surface (Chen *et al.* 2021a). As the ozone dosage gradually increased, the contact between ozone molecules and the catalyst increased, and the amount of ·OH generated in the system gradually increased, thereby increasing the COD removal from the ROC. When the ozone dosage was gradually increased to 1.0 g/L, the

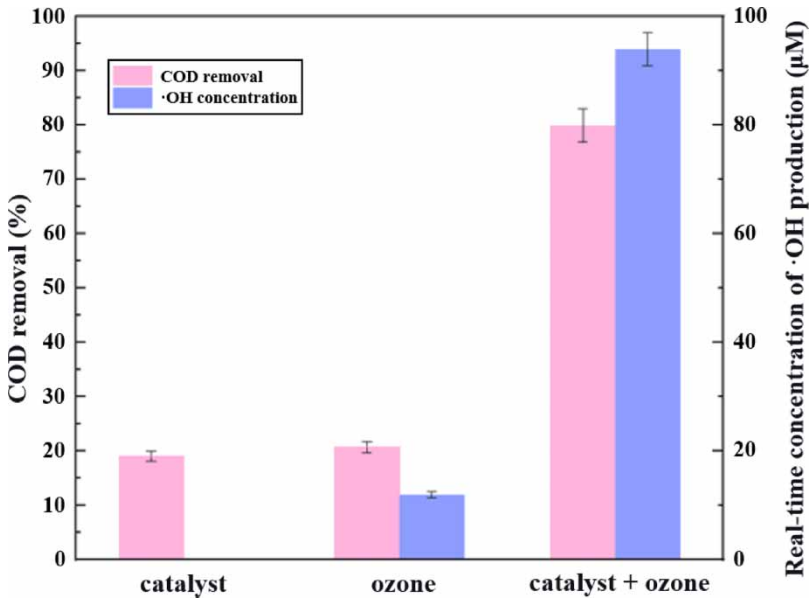

Figure 4 | COD removal and real-time concentration of ·OH production of 'Cu-Co-Mn/AC', 'Ozone', and 'Cu-Co-Mn/AC + ozone'.

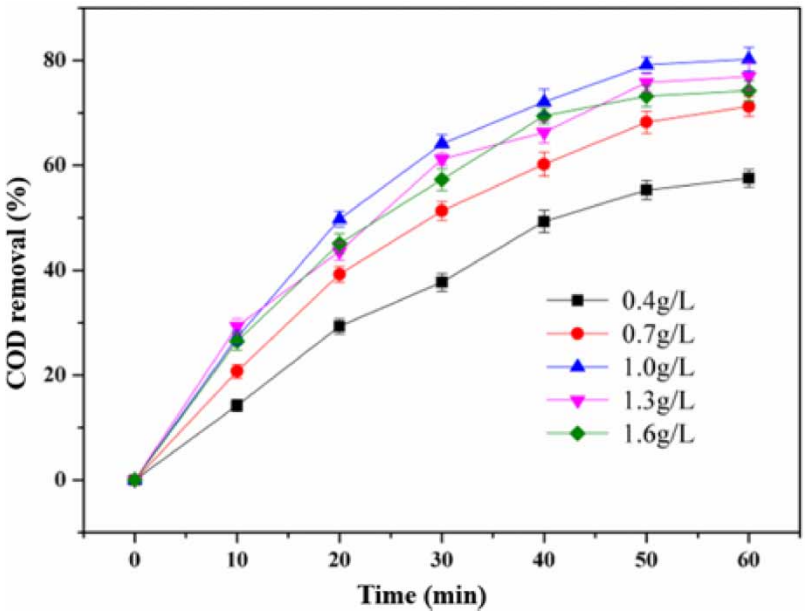

Figure 5 | Effect of different ozone dosages on the catalytic oxidation performance (catalyst dosage = 1.20 g/L, initial pH = 9, t = 60 min).

Cu-Co-Mn/AC catalytic ozone oxidation had the best performance in the treatment of ROC, and the COD removal reached 80.23%. When the ozone dosage was further increased, the catalytic ozonation performance worsened. If the catalyst dosage remained constant, the increasing ozone dosage would saturate the active sites on the catalyst's surface (Chen & Wang 2019). The decomposition of ozone was restricted, and the solution contained excess ozone molecules, which react with ·OH in the system and affect the reaction between ·OH and organic compounds (Kusic *et al.* 2006). ·OH was gradually consumed, thereby decreasing its content in the solution and the COD removal from the ROC.

3.3.2. Effect of catalyst dosage

The removal of COD gradually stabilised as the reaction time reached 60 min, when the catalyst dosage determined the final COD removal of the reaction system. As shown in Figure 6, when the catalyst dosage was quite low, it was insufficient to

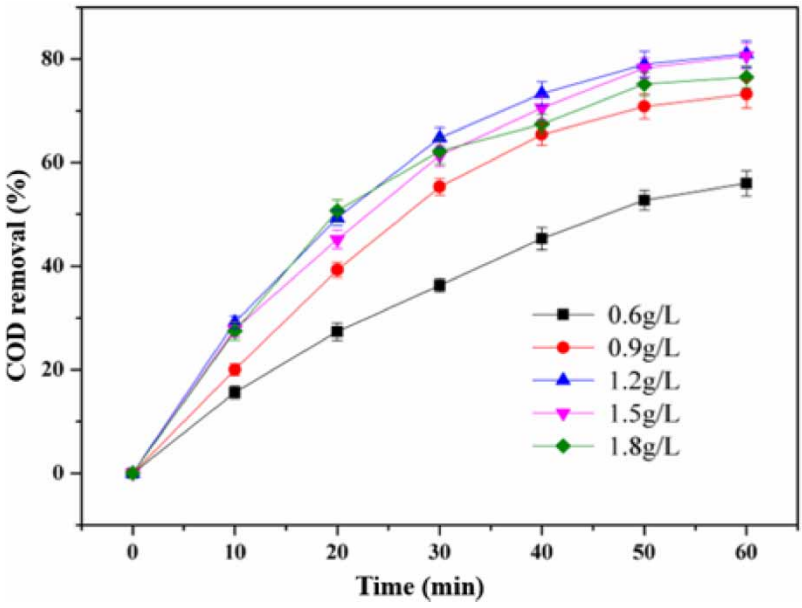

Figure 6 | Effect of different catalyst dosages on the catalytic oxidation performance (ozone dosage = 1.0 g/L, pH = 9, t = 60 min).

catalyse the decomposition of most of the ozone in the system, and the amount of ·OH that reacted in the solution remained low. The adsorption of catalysts can also remove pollutants (Gupta *et al.* 2018). Here, a small number of catalysts adsorbed a small amount of organic matter, resulting in insufficient removal of COD from the concentrate. As the catalyst dosage gradually increased, the number of active sites for catalytic ozone oxidation increased (Fan *et al.* 2021). The amount of ·OH generated in the solution also gradually increased, thereby increasing the removal of COD. When the catalyst dosage reached 1.2 g/L, the Cu-Co-Mn/AC catalytic ozonation process achieved the best performance in the treatment of COD, and the COD removal reached 80.61%. The final COD removal decreased slightly as the catalyst dosage further increased, which was due to the self-quenching reaction of ·OH with high concentrations (Lucas *et al.* 2010; Jiao *et al.* 2015). When the ozone concentration of the reaction system remained constant, the addition of more catalysts could accelerate the decomposition of ozone (Patil *et al.* 2020), leading to a rapid increase in the ·OH concentration of the aqueous solution per unit time and causing the excess ·OH in the solution to consume one another. The amount of ·OH that participated in the oxidation of organic matter declined, ultimately causing a decline in COD removal. However, the three curves of '1.2 $g{\cdot}L^{-1}$', '1.5 $g{\cdot}L^{-1}$', and '1.8 $g{\cdot}L^{-1}$' indicated that the decline in COD removal was within 5 as the COD removed by adsorption increased, which offset the effect of ·OH self-quenching.

3.3.3. Effect of initial pH

As shown in Figure 7, when the initial environment of the reaction system was acidic, the performance of the Cu-Co-Mn/AC catalytic ozonation was poor as acidic conditions are not conducive to the decomposition of ozone (Malik *et al.* 2020), i.e., the generation of ·OH was hindered. At this time, the removal of COD mainly relied on the direct oxidation of ozone, and the oxidation performance of ozone was poorer than that of ·OH (Chen *et al.* 2021b), resulting in a lower COD removal. During the initial stage of the reaction, catalytic ozonation achieved better COD removal under neutral or alkaline conditions. As the initial pH gradually increased, the amount of OH^- in the system gradually increased, which could promote the decomposition reaction of ozone (Lin *et al.* 2009). More ·OH was generated, causing the removal of COD to gradually increase. However, as the reaction progressed, the pH of the system gradually decreased, and the catalytic ozonation was hindered. This could be the reason for the better final COD removal at an initial pH of 9 or 11 than that at an initial pH of 7. The Cu-Co-MN/AC catalytic ozonation system achieved the best COD removal of 80.94% at an initial pH of 9. When the initial pH was increased to 11, the final COD removal declined. The reason for this was the same as that described in Section 3.3.2,

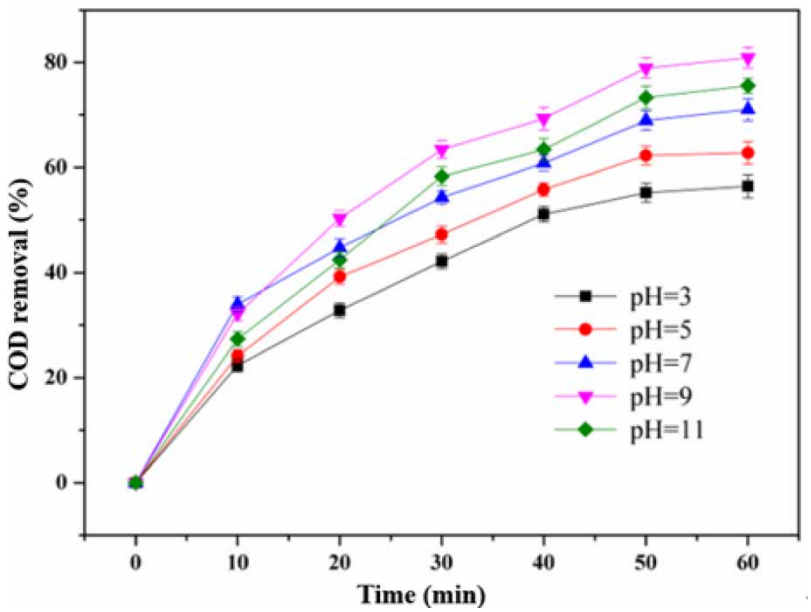

Figure 7 | Effect of different initial pH on the catalytic oxidation performance (ozone dosage = 1.0 g/L, catalyst dosage = 1.20 g/L, t = 60 min).

i.e., excess ·OH generated in the solution underwent a self-quenching reaction, causing the ·OH content of the system to decline; thus, decreasing the final removal of COD.

Additionally, the presence of a large amount of Cl^- in the concentrate affected the oxidation effect and COD removal, as it could react with ozone under acidic conditions (Levanov *et al.* 2018; Yuan *et al.* 2022), depleting the ozone in the system. At the same time, it was found that an increase in the Cl^- concentration led to a decline in the ·OH concentration; however, at a higher Cl^- concentration, regardless of how it changed, the ·OH concentration remained constant, and increasing the pH could offset the effect of the increasing Cl^- concentration on the removal of organic matter (Liao *et al.* 2001). Therefore, under neutral or alkaline conditions, catalytic ozone oxidation achieved a significantly better COD removal effect from ROC.

3.4. Response surface model for optimising the reaction parameters

3.4.1. Design and results of response surface experiments

An RSM was used to simulate and verify the optimal reaction conditions for the catalytic ozonation system. The initial pH, ozone dosage, and catalyst dosage were studied in the experiment. According to the results of the single factor experiments described in Section 3.3, the initial pH, ozone dosage, and catalyst dosage were set to 7–11, 0.7–1.3 g/L, and 0.9–1.5 g/L, respectively, and the reaction time was set to 60 min. The three-factor and three-level tests were designed according to the Box-Benhken design (BBD) method, and the distribution of each variable is listed in Table 3. A response surface experiment with 17 points was also designed according to the BBD method. The zero experiment was conducted five times to estimate the error of the experiment, and response surface analysis was conducted on the data in Table 4 using Design-Expert 8.0.6 to obtain the second-order polynomial equation of COD removal, as described in Equation (1):

$$Y = 80.13 + 2.09X_1 + 3.06X_2 + 4.53X_3 - 2.35X_1X_2 - 2.96X_1X_3 - 1.24X_2X_3 - 7.72X_1^2 - 4.82X_2^2 - 4.67X_3^2 \quad (1)$$

3.4.2. Analysis of variance and significance test

Table 5 shows the results of the ANOVA analysis of the RSM. The F-value represents the ratio of the mean square error of the model to the error, and the *p*-value represents the probability of an impossible event in the model. A model with a large F-value and small *p*-value is more significant (Das & Goud 2021). The F-value of this model was 44.39, and *p*-value was <0.0001, indicating that the model was highly significant. Additionally, the lack-of-fit item had F and *p*-values of 5.99 and 0.0582 (not significant), respectively.

Table 6 shows the reliability analysis parameters of the RSM. The value of R^2 reflects how well the model fits the corresponding data (Abdulkadir *et al.* 2021). The correlation coefficient R^2 of the model was approximately 0.9828, indicating that the coincidence of this RSM to a series of experiments reached 98.28%, and the fit was good. The square values of the modified negative correlation coefficient Adj R-Squared was 0.9606, and the square values of the predicted negative correlation coefficient Pred R-Squared was 0.7697. (Adj R-Squared) – (Pred R-Squared) $= 0.1909 < 2$, indicating that the model fitted the experimental process well. CV% $= 1.9970\% < 10\%$, indicating high reliability. The signal-to-noise ratio Adeq Precision $= 19.9294 > 4$, indicating that the experimental results predicted by the model were accurate.

Figure 8 shows the residual plot of the RSM. Figure 8(a) shows the probability distribution diagram of the residual errors. The relevant numerical values were fitted to a straight line, and were evenly distributed, indicating that it is reasonable to select COD removal as the response value of the model. Figure 8(b) compares the predicted and simulated values, and their linear distribution indicates that they were similar. Figure 8(c) shows the relationship between the internalised residual

Table 3 | Distribution of each variable

Variate	Factor	Unit	Range and level		
			−1	0	1
X_1	pH	–	7	9	11
X_2	Ozone dosage	$g{\cdot}L^{-1}$	0.7	1.0	1.3
X_3	Catalyst dosage	$g{\cdot}L^{-1}$	0.9	1.2	1.5

Table 4 | RSM experimental scheme and results

	Factors			
Run	X_1	X_2	X_3	*Y*: COD removal (%)
1	0	0	0	79.89
2	1	−1	0	67.23
3	0	1	1	76.34
4	0	0	0	80.72
5	1	0	1	72.13
6	0	−1	1	74.21
7	0	0	0	79.78
8	1	1	0	70.13
9	−1	0	−1	57.32
10	0	0	0	81.01
11	−1	−1	0	60.23
12	−1	0	1	71.97
13	0	0	0	78.97
14	0	1	−1	69.45
15	0	−1	−1	62.34
16	1	0	−1	69.32
17	−1	1	0	72.54

Table 5 | ANOVA of the RSM

Source	Sum of squares	df	Mean square	F value	*p*-value Prob > F
Model	825.42	9	91.71	44.39	<0.0001
X_1	35.07	1	35.07	16.97	0.0045
X_2	74.73	1	74.73	36.17	0.0005
X_3	163.99	1	163.99	79.37	<0.0001
X_1X_2	22.14	1	22.14	10.71	0.0136
X_1X_3	35.05	1	35.05	16.96	0.0045
X_2X_3	6.20	1	6.20	3.00	0.1268
X_1^2	250.99	1	250.99	121.49	<0.0001
X_2^2	97.85	1	97.85	47.36	0.0002
X_3^2	91.76	1	91.76	44.41	0.0003
Residual	14.46	7	2.07		
Lack of Fit	11.83	3	3.94	5.99	0.0582
Pure Error	2.63	4	0.66		
Cor Total	839.88	16			

and predicted value. The values were distributed randomly, indicating that the model was credible. Finally, Figure 8(d) shows the relationship between the internalised residual error and experiment number. The overall irregular distribution indicates that there was no correlation between the experimental results and number. In summary, the RSM could simulate the effects of the initial pH, ozone dosage, and catalyst dosage on the COD removal of the concentrate.

Table 6 | Reliability analysis of the RSM

Parameter	Value	Parameter	Value
Std. Dev.	1.43735844	R-Squared	0.982780966
Mean	71.97529412	Adj R-Squared	0.960642208
C.V. %	1.997016418	Pred R-Squared	0.769748131
PRESS	193.3849125	Adeq Precision	19.92940698

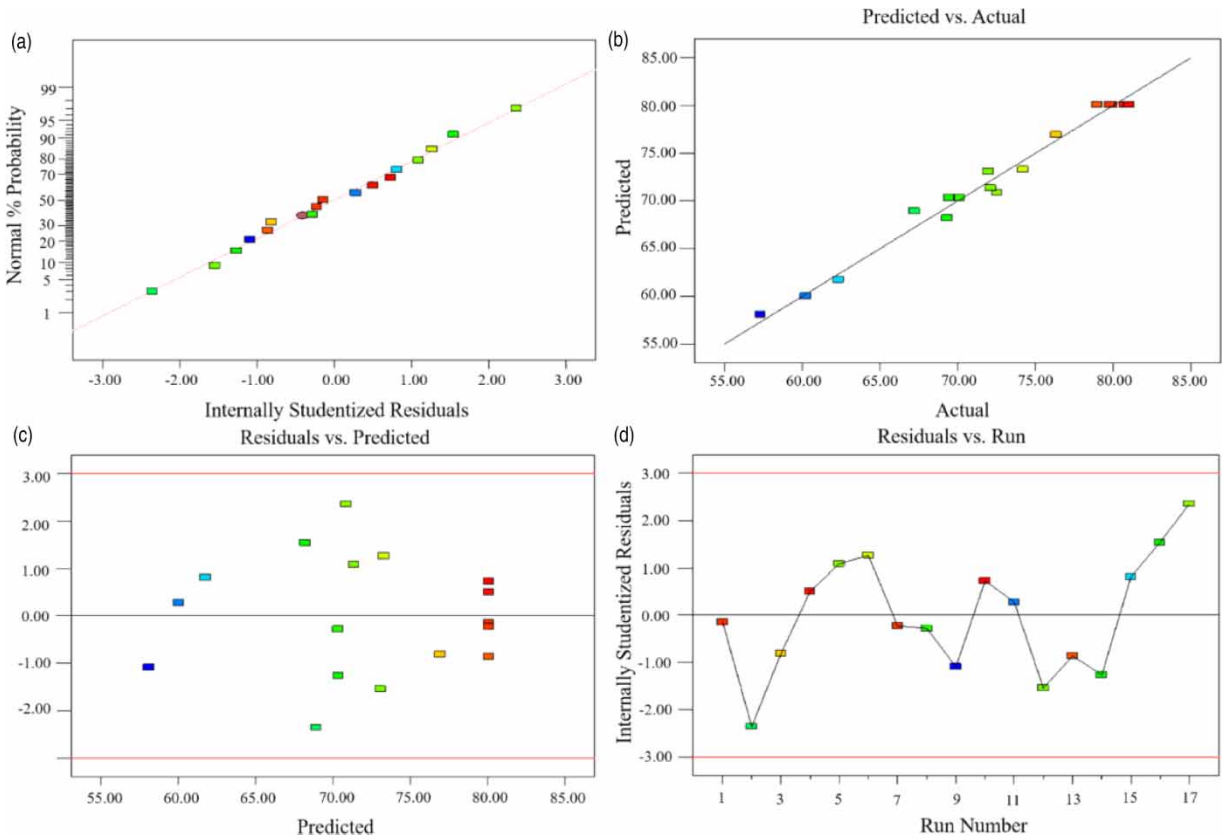

Figure 8 | Residual diagram of the RSM.

3.4.3. Process parameter optimisation

First, we analysed the degree of influence of the initial pH, ozone dosage, and catalyst dosage on COD removal. A larger F-value indicates that the parameter is more important (Chen *et al.* 2021c). Table 5 indicates that the F-values of the three variables (X_1, X_2, and X_3) were 16.97, 36.17, and 79.37, respectively. The strength of the influence of the three variables on the response value decreased in the following order: $X_3 > X_2 > X_1$; i.e., when the removal of COD from the concentrate was used as the response value, the catalyst dosage had the greatest impact, followed by the ozone dosage and initial pH. From Table 5, the significant items for the response value Y can also be filtered out, which were X_1, X_2, X_3, X_1X_3, X_{12}, X_{22}, and X_{32}. After selectively removing insignificant terms, the second-order polynomial can be simplified as Equation (2):

$$Y = 80.13 + 2.09X_1 + 3.06X_2 + 4.53X_3 - 2.96X_1X_3 - 7.72X_1^2 - 4.82X_2^2 - 4.67X_3^2 \quad (2)$$

The maximum COD removal predicted by the RSM was 81.49%, and the corresponding reaction conditions were as follows: pH = 9.02, ozone dosage = 1.08 g/L, catalyst dosage = 1.33 g/L. The reaction conditions determined in Section 3.3

were as follows: pH = 9.00, ozone dosage = 1.00 g/L, and catalyst dosage = 1.20 g/L, and the COD removal was 80.94%. Therefore, the modelled and experimentally determined reaction conditions were very similar, indicating that the model was suitable.

4. CONCLUSIONS

The Cu-Co-Mn/AC catalyst was prepared to enhance the ozonation performance in treating refractory organics in the ROC. The presence of the Cu-Co-Mn/AC catalyst promoted the decomposition of ozone to generate ·OH in the solution. It was shown in the univariate analysis that ozone dosage, catalyst dosage, and pH affect the COD removal in the ROC by affecting the generation of ·OH. In the RSM, COD removal was the dependent variable Y, and the optimal conditions were an ozone dosage of 1.08 g/L, a catalyst dosage of 1.33 g/L, and a pH of 9.02. Moreover, the catalyst dosage had a significant impact on COD removal, for it provided active sites for ozone decomposition to generate ·OH. Thus, this study provided a feasible approach for enhancing the removal performance of refractory organic compounds in ROC via Cu-Co-Mn/AC catalytic ozonation.

ACKNOWLEDGEMENT

This research was supported by the National Key Research and Development Program of China (2019YFC1806104, 2017YFB0602804), and the National Natural Science Foundation (51378207).

DATA AVAILABILITY STATEMENT

All relevant data are included in the paper or its Supplementary Information.

CONFLICT OF INTEREST

The authors declare there is no conflict.

REFERENCES

Abdulkadir, I., Mohammed, B. S., Liew, M. S. & Wahab, M. M. A. 2021 Modelling and multi-objective optimization of the fresh and mechanical properties of self-compacting high volume fly ash ECC (HVFA-ECC) using response surface methodology (RSM). *Case Studies in Construction Materials* **14**. https://doi.org/10.1016/j.cscm.2021.e00525.

Aldeguer Esquerdo, A., Sentana Gadea, I., Varo Galvan, P. J. & Prats Rico, D. 2021 Efficacy of atrazine pesticide reduction in aqueous solution using activated carbon, ozone and a combination of both. *Science of the Total Environment* **764**. https://doi.org/10.1016/j.scitotenv.2020.144301.

Araújo, A., Soares, O. S. G. P., Orge, C. A., Gonçalves, A. G., Rombi, E., Cutrufello, M. G., Fonseca, A. M., Pereira, M. F. R. & Neves, I. C. 2021 Metal-zeolite catalysts for the removal of pharmaceutical pollutants in water by catalytic ozonation. *Journal of Environmental Chemical Engineering* **9** (6). https://doi.org/10.1016/j.jece.2021.106458.

Chen, H. & Wang, J. 2019 Catalytic ozonation of sulfamethoxazole over Fe_3O_4/Co_3O_4 composites. *Chemosphere* **234**, 14–24. https://doi.org/10.1016/j.chemosphere.2019.06.014.

Chen, H. & Wang, J. 2021 Catalytic ozonation for degradation of sulfamethazine using $NiCo_2O_4$ as catalyst. *Chemosphere* **268**. https://doi.org/10.1016/j.chemosphere.2020.128840.

Chen, Y., Li, S. & Hu, J. 2020 Photoelectrocatalytic degradation of organics and formation of disinfection byproducts in reverse osmosis concentrate. *Water Research* **168**, 115105. https://doi.org/10.1016/j.watres.2019.115105.

Chen, H., Zhang, Z., Hu, D., Chen, C., Zhang, Y., He, S. & Wang, J. 2021a Catalytic ozonation of norfloxacin using co3o4/C composite derived from ZIF-67 as catalyst. *Chemosphere* **265**. https://doi.org/10.1016/j.chemosphere.2020.129047.

Chen, L., Wang, H., Sun, Y., Zhao, Y. & Shi, H. 2021b Interface mechanisms of the catalytic ozonation of humic acids over siliceous ferrihydrite: morphology, stability, and the catalytic process. *Environmental Reseach* **203**. https://doi.org/10.1016/j.envres.2021.111870.

Chen, W.-H., Chiu, G.-L., Chyuan Ong, H., Shiung Lam, S., Lim, S., Sik Ok, Y. & Kwon, E. 2021c Optimization and analysis of syngas production from methane and CO2 via Taguchi approach, response surface methodology (RSM) and analysis of variance (ANOVA). *Fuel* **296**. https://doi.org/10.1016/j.fuel.2021.120642.

Das, S. & Goud, V. V. 2021 RSM-optimised slow pyrolysis of rice husk for bio-oil production and its upgradation. *Energy* **225**. https://doi.org/10.1016/j.energy.2021.120161.

Fan, S., Song, J., Xia, Y. & Dai, Q. 2021 Catalytic ozonation of thymol with a novel CoCe-MMO catalyst: kinetics and mechanism. *Environmental Technology & Innovation* **24**. https://doi.org/10.1016/j.eti.2021.101881.

Gupta, V. K., Fakhri, A., Agarwal, S., Bharti, A. K., Naji, M. & Tkachev, A. G. 2018 Preparation and characterization of TiO 2 nanofibers by hydrothermal method for removal of Benzodiazepines (Diazepam) from liquids as catalytic ozonation and adsorption processes. *Journal of Molecular Liquids* **249**, 1033–1038. https://doi.org/10.1016/j.molliq.2017.11.144.

He, C., Wang, J., Wang, C., Zhang, C., Hou, P. & Xu, X. 2020 Catalytic ozonation of bio-treated coking wastewater in continuous pilot- and full-scale system: efficiency, catalyst deactivation and in-situ regeneration. *Water Research* **183**, 116090. https://doi.org/10.1016/j.watres.2020.116090.

Hou, S., Jia, S., Jia, J., He, Z., Li, G., Zuo, Q. & Zhuang, H. 2020 Fe3o4 nanoparticles loading on cow dung based activated carbon as an efficient catalyst for catalytic microbubble ozonation of biologically pretreated coal gasification wastewater. *Journal of Environmental Management* **267**, 110615. https://doi.org/10.1016/j.jenvman.2020.110615.

Huang, Y., Yang, T., Liang, M., Wang, Y., Xu, Z., Zhang, D. & Li, L. 2019 Ni-Fe layered double hydroxides catalized ozonation of synthetic wastewater containing Bisphenol A and municipal secondary effluent. *Chemosphere* **235**, 143–152. https://doi.org/10.1016/j.chemosphere.2019.06.162.

Jia, S., Han, Y., Zhuang, H., Han, H. & Li, K. 2017 Simultaneous removal of organic matter and salt ions from coal gasification wastewater RO concentrate and microorganisms succession in a MBR. *Bioresource Technology* **241**, 517–524. https://doi.org/10.1016/j.biortech.2017.05.158.

Jiao, W., Yu, L., Feng, Z., Guo, L., Wang, Y. & Liu, Y. 2015 Optimization of nitrobenzene wastewater treatment with O3/h2o2in a rotating packed bed using response surface methodology. *Desalination and Water Treatment* **57** (42), 19996–20004. https://doi.org/10.1080/19443994.2015.1102771.

Keyikoglu, R., Karatas, O., Rezania, H., Kobya, M., Vatanpour, V. & Khataee, A. 2021 A review on treatment of membrane concentrates generated from landfill leachate treatment processes. *Separation and Purification Technology* **259**. https://doi.org/10.1016/j.seppur.2020.118182.

Kusic, H., Koprivanac, N. & Bozic, A. L. 2006 Minimization of organic pollutant content in aqueous solution by means of AOPs: UV- and ozone-based technologies. *Chemical Engineering Journal* **123** (3), 127–137. https://doi.org/10.1016/j.cej.2006.07.011.

Levanov, A. V., Isaikina, O. Y., Gasanova, R. B. & Lunin, V. V. 2018 Solubility of ozone and kinetics of its decomposition in aqueous chloride solutions. *Industrial & Engineering Chemistry Research* **57** (43), 14355–14364. https://doi.org/10.1021/acs.iecr.8b03371.

Li, Y., Li, M., Xiao, K. & Huang, X. 2020 Reverse osmosis membrane autopsy in coal chemical wastewater treatment: evidences of spatially heterogeneous fouling and organic-inorganic synergistic effect. *Journal of Cleaner Production* **246**. https://doi.org/10.1016/j.jclepro.2019.118964.

Li, P., Miao, R., Wang, P., Sun, F. & Li, X.-y. 2021 Bi-metal oxide-modified flat-sheet ceramic membranes for catalytic ozonation of organic pollutants in wastewater treatment. *Chemical Engineering Journal* **426**. https://doi.org/10.1016/j.cej.2021.131263.

Liao, C.-H., Kang, S.-F. & Wu, F.-A. 2001 Hydroxyl radical scavenging role of chloride and bicarbonate ions in the H_2O_2/UV process. *Chemosphere* **44**, 1193–1200.

Lin, C. C., Chao, C. Y., Liu, M. Y. & Lee, Y. L. 2009 Feasibility of ozone absorption by H_2O_2 solution in rotating packed beds. *Journal of Hazardous Materials* **167** (1–3), 1014–1020. https://doi.org/10.1016/j.jhazmat.2009.01.092.

Liu, Z. Q., You, L., Xiong, X., Wang, Q., Yan, Y., Tu, J., Cui, Y. H., Li, X. Y., Wen, G. & Wu, X. 2019 Potential of the integration of coagulation and ozonation as a pretreatment of reverse osmosis concentrate from coal gasification wastewater reclamation. *Chemosphere* **222**, 696–704. https://doi.org/10.1016/j.chemosphere.2019.01.187.

Liu, Z.-Q., Huang, C., Li, J.-Y., Yang, J., Qu, B., Yang, S.-Q., Cui, Y.-H., Yan, Y., Sun, S. & Wu, X. 2021 Activated carbon catalytic ozonation of reverse osmosis concentrate after coagulation pretreatment from coal gasification wastewater reclamation for zero liquid discharge. *Journal of Cleaner Production* **286**. https://doi.org/10.1016/j.jclepro.2020.124951.

Lucas, M. S., Peres, J. A. & Li Puma, G. 2010 Treatment of winery wastewater by ozone-based advanced oxidation processes (O3, O3/UV and O3/UV/H2O2) in a pilot-scale bubble column reactor and process economics. *Separation and Purification Technology* **72** (3), 235–241. https://doi.org/10.1016/j.seppur.2010.01.016.

Luo, Z., Wang, D., Zeng, W. & Yang, J. 2020 Removal of refractory organics from piggery bio-treatment effluent by the catalytic ozonation process with piggery biogas residue biochar as the catalyst. *Science of the Total Environment* **734**, 139448. https://doi.org/10.1016/j.scitotenv.2020.139448.

Malik, S. N., Ghosh, P. C., Vaidya, A. N. & Mudliar, S. N. 2020 Hybrid ozonation process for industrial wastewater treatment: principles and applications: a review. *Journal of Water Process Engineering* **35**. https://doi.org/10.1016/j.jwpe.2020.101193

Nakhate, P. H., Gadipelly, C. R., Joshi, N. T. & Marathe, K. V. 2019 Engineering aspects of catalytic ozonation for purification of real textile industry wastewater at the pilot scale. *Journal of Industrial and Engineering Chemistry* **69**, 77–89. https://doi.org/10.1016/j.jiec.2018.09.010.

Nawrocki, J. & Kasprzyk-Hordern, B. 2010 The efficiency and mechanisms of catalytic ozonation. *Applied Catalysis B: Environmental* **99** (1–2), 27–42. https://doi.org/10.1016/j.apcatb.2010.06.033.

Patil, V. V., Gogate, P. R., Bhat, A. P. & Ghosh, P. K. 2020 Treatment of laundry wastewater containing residual surfactants using combined approaches based on ozone, catalyst and cavitation. *Separation and Purification Technology* **239**. https://doi.org/10.1016/j.seppur.2020.116594

Shi, J., Huang, W., Han, H. & Xu, C. 2020 Review on treatment technology of salt wastewater in coal chemical industry of China. *Desalination* **493**. https://doi.org/10.1016/j.desal.2020.114640.

Valdes, H. & Zaror, C. A. 2006 Heterogeneous and homogeneous catalytic ozonation of benzothiazole promoted by activated carbon: kinetic approach. *Chemosphere* **65** (7), 1131–1136. https://doi.org/10.1016/j.chemosphere.2006.04.027.

Wang, Y., Wang, J., Liu, L., Cao, Z., Wang, J., Jia, M. & Ji, X. 2021 Treatment of coal gasification brine by membrane distillation: effect of mixed fouling and pretreatment on process performance. *Desalination* **499**. https://doi.org/10.1016/j.desal.2020.114820.

Westerhoff, P., Moon, H., Minakata, D. & Crittenden, J. 2009 Oxidation of organics in retentates from reverse osmosis wastewater reuse facilities. *Water Research* **43** (16), 3992–3998. https://doi.org/10.1016/j.watres.2009.04.010.

Yang, L., Sheng, M., Li, Y., Xue, W., Li, K. & Cao, G. 2020 A hybrid process of Fe-based catalytic ozonation and biodegradation for the treatment of industrial wastewater reverse osmosis concentrate. *Chemosphere* **238**, 124639. https://doi.org/10.1016/j.chemosphere.2019.124639.

Yang, J., Hou, Z., Chen, Z., Ma, Z., Li, S., Wang, Y., Gao, J. & Cui, P. 2021 Comprehensive analysis of diverse biochemical treatment technologies of fixed-bed coal gasification wastewater from the perspective of different weight dimensions. *Separation and Purification Technology* **257**. https://doi.org/10.1016/j.seppur.2020.117889.

Yuan, Y., Xing, G., Garg, S., Ma, J., Kong, X., Dai, P. & Waite, T. D. 2020 Mechanistic insights into the catalytic ozonation process using iron oxide-impregnated activated carbon. *Water Research* **177**, 115785. https://doi.org/10.1016/j.watres.2020.115785.

Yuan, Y., Garg, S., Wang, Y., Li, W., Chen, G., Gao, M., Zhong, J., Wang, J. & Waite, T. D. 2022 Influence of salinity on the heterogeneous catalytic ozonation process: implications to treatment of high salinity wastewater. *Journal of Hazardous Materials* **423**. https://doi.org/10.1016/j.jhazmat.2021.127255.

Zhou, L., Zhang, S., Li, Z., Liang, X., Zhang, Z., Liu, R. & Yun, J. 2020 Efficient degradation of phenol in aqueous solution by catalytic ozonation over MgO/AC. *Journal of Water Process Engineering* **36**. https://doi.org/10.1016/j.jwpe.2020.101168.

Zhu, H., Han, Y., Xu, C., Han, H. & Ma, W. 2018 Overview of the state of the art of processes and technical bottlenecks for coal gasification wastewater treatment. *Science of the Total Environment* **637–638**, 1108–1126. https://doi.org/10.1016/j.scitotenv.2018.05.054.

First received 21 August 2022; accepted in revised form 13 December 2022. Available online 21 December 2022